

Structure and Functionality of a Designed p53 Dimer

Timothy S. Davison¹, X. Nie¹, Weili Ma¹, Yunping Lin¹, C. Kay²
S. Benchimol¹ and Cheryl H. Arrowsmith^{1*}

¹Ontario Cancer Institute and
Department of Medical
Biophysics, University of
Toronto, 610 University Ave.
Toronto, Ontario, Canada
M5G 2M9

²Department of Biochemistry
University of Alberta
Edmonton, Alberta, Canada
T6G 2H7

P53 is a homotetrameric tumor suppressor protein involved in transcriptional control of genes that regulate cell proliferation and death. In order to probe the role that oligomerization plays in this capacity, we have previously designed and characterized a series of p53 proteins with altered oligomeric states through hydrophilic substitution of residues Met340 or Leu344 in the normally tetrameric oligomerization domain. Although such mutations have little effect on the overall secondary structural content of the oligomerization domain, both solubility and the resistance to thermal denaturation are substantially reduced relative to that of the wild-type domain. Here, we report the design and characterization of a double-mutant p53 with alterations of residues at positions Met340 and Leu344. The double-mutations Met340Glu/Leu344Lys and Met340Gln/Leu344Arg resulted in distinct dimeric forms of the protein. Furthermore, we have verified by NMR structure determination that the double-mutant Met340Gln/Leu344Arg is essentially a “half-tetramer”. Analysis of the *in vivo* activities of full-length p53 oligomeric mutants reveals that while cell-cycle arrest requires tetrameric p53, transcriptional transactivation activity of monomers and dimers retain roughly background and half of the wild-type activity, respectively.

© 2001 Academic Press

Keywords: p53 dimer; oligomerization; NMR; cell cycle arrest; transcriptional transactivation

*Corresponding author

Introduction

Wild-type p53 (Wtp53) is a homotetrameric nuclear phosphoprotein that functions as a tumor suppressor.^{1,2} p53 can induce growth arrest or apoptosis in response to DNA damage through its role as a transcriptional regulator of genes involved in cell-cycle control^{3–6} and apoptosis.^{7,8} Inactivation of p53 through deletion, mutation or interaction with viral or cellular proteins is a fundamental step in the development of over half of all human cancers.^{9–11} Like many transcription factors, p53 is a modular protein composed of an N-terminal activation domain, a central DNA-

binding domain, a tetramerization domain and a C-terminal regulatory region.^{10–12}

The vast majority of sporadic tumor-derived or germline-related p53 mutations are found within the core DNA-binding domain.^{13–16} Relatively few missense mutations are found within the tetramerization domain (p53tet),¹³ suggesting that either (i) p53tet is less sensitive to mutations than the core domain,^{17–20} (ii) tetramerization is not essential for tumor suppression,^{21–23} or (iii) an intact tetramerization domain is selected for in tumorigenesis²⁴ in order to mediate the dominant negative activity of DNA-binding mutants.²⁵ In contrast to hypothesis (i), both the stability and oligomerization of p53tet appear to be quite sensitive to mutation.²⁶ Furthermore, several recent studies have uncovered inherited germline mutations in the tetramerization domain (Arg337Cys and Leu344Pro) of individuals with Li-Fraumeni (LFS) and Li-Fraumeni-like (LFL) syndromes.^{27,28} These syndromes are characterized by increased susceptibility of affected individuals to a specific spectrum of cancers (including breast and brain cancers, sarcomas, and leukemia) at an early age, often associated with a germline mutation in p53 or regulators of the p53 pathway

Abbreviations used: BSA, bovine serum albumin; CD, circular dichroism; FITC, fluorescein isothiocyanate; LFL, Li-Fraumeni-like syndrome; LFS, Li-Fraumeni syndrome; NCS, non-crystallographic symmetry; NMR, nuclear magnetic resonance; NOE, nuclear Overhauser effect; PBS, phosphate-buffered saline; 3D, three-dimensional; WT, wild-type; PDB, protein data bank; RCSB, research collaborative for structural bioinformatics; BMRB, BioMagResBank.

E-mail address of the corresponding author:
carrow@oci.utoronto.ca

such as Chk2.²⁹ We have previously shown that these two mutations lead to partial (Arg337Cys) and complete (Leu344Pro) abrogation of the ability of p53 to oligomerize.³⁰ Because individuals with these mutations developed LFS and LFL, this suggests that even partial disruption of p53 oligomerization can contribute to a loss of tumor suppressor function that may in turn accelerate the process of tumorigenesis.

In order to probe the role of oligomerization in the function of p53, we designed a series of single³¹ and double p53tet mutants with altered oligomeric states. In particular, we generated a dimeric form of p53 (a half-tetramer) which was designed to retain the relative orientations of the p53 domains N and C-terminal to the tetramerization domain. This may be important for maintaining regulatory aspects of the full-length p53 protein.

Here, we report the 3D structure of this dimeric p53 oligomerization domain, as well as the functional characterization of a series of p53tet mutants with altered oligomeric states. The results provide insight into the role that oligomerization plays in p53's capacity as a tumor suppressor protein.

Results

Structure-based design of p53 mutants with altered oligomeric states

The p53 tetramerization domain is a symmetric dimer of dimers.^{19,32–34} Each dimer contains an antiparallel β -sheet packed against a pair of antiparallel α -helices. The two dimers associate in a roughly orthogonal manner to form a four-helix bundle sandwiched between two pairs of β -sheets. The hydrophobic core is comprised of two spatially separated regions: a small core within each of the two symmetric dimers and an extensive (2006 Å²) hydrophobic patch at the dimer-dimer interface (Figure 1(a) and (b)). In order to generate dimeric mutants, residues Met340 and Leu344 were targeted for mutation due to their central role in the formation of the dimer-dimer interface.²⁶ A series of hydrophilic residues with high α -helical propensities (Lys, Arg, Glu, Asp, Gln, Ser and His) were chosen as candidates for substitution at positions 340 and/or 344. Due to the quaternary organization of the oligomerization domain, a single amino acid mutation will introduce four hydrophilic residues into the dimer-dimer interface (Figure 1(c)). Similarly, a double mutation introduces eight hydrophilic residues into the interface (Figure 1(d)). The subsequent reduction of the hydrophobic interface of each dimer should destabilize or inhibit interaction between two dimers while enhancing the solubility of an individual dimer.

In order to identify the effects of non-conservative substitutions within the dimer-dimer interface, each of the p53tet mutants was assayed for: (i) solubility; (ii) secondary structural content; (iii) resistance to thermal denaturation; and (iv) oligo-

meric state. Since our aim was to study the structural differences and *in vivo* functionality of a stable, dimeric form of p53, these experiments facilitated the identification of suitable mutants for further structural characterization by NMR spectroscopy, transcriptional transactivation and cell-cycle arrest assays.

Oligomeric mutants display a range of propensities to aggregate

Due to the nature of the non-conservative mutations within the hydrophobic dimer-dimer interface, it was plausible that the quaternary organization of the domain would be altered. In a first screening of the mutants, each protein sample was concentrated to 250 μ M and the near-UV spectrum was analyzed for characteristics of aggregation. Due to the presence of significant Rayleigh scattering, it was apparent that a number of single-mutants at position 340 contained a significant proportion of large, soluble aggregates (data not shown). To better quantify the extent of aggregation, each sample was filtered through low protein-binding 0.22 μ m membranes (Millipore), and the UV absorbance at 275 nm was compared to the pre-filtered absorbance. Furthermore, pre and post-filtered samples were analyzed by SDS-PAGE to verify the proportion of protein retained by the membrane. These experiments indicate that samples of mutants Met340His, Met340Ser, Met340Asp and Met340Glu are predominantly aggregated ($\geq 45\%$), while Met340Gln and Leu344Ala display moderate aggregation with a loss of 25% to 50% of UV absorbance signal. The remaining mutants and WT samples show little or no loss of UV signal post-filtration (see Table 1). In order to identify potential candidates for NMR structural analysis, we attempted to concentrate each mutant to a minimum concentration of 1 mM. While the single-mutants Leu344Lys and Leu344Arg could be concentrated to this lower concentration limit, only the double mutants Met340Gln/Leu344Arg (MQLR) and Met340Glu/Leu344Lys (MELK) could be concentrated to levels ≥ 1.5 mM without the appearance of soluble aggregates. The 2 mM samples of MQLR and MELK were further subjected to sedimentation equilibrium analytical ultracentrifugation, which verified its dimeric state and lack of aggregation at NMR concentrations (data not shown).

Oligomeric mutants retain wild-type secondary structure but are destabilized relative to WTp53

To assess the effect of mutation on the secondary structural content, each mutant was analyzed by far-UV circular dichroism spectroscopy (CD). A comparison of the CD signals indicates that there is no measurable change in the total secondary structure of each mutant within experimental error (Figure 2(a)). While each of the mutants retains the secondary structure of WT p53tet,

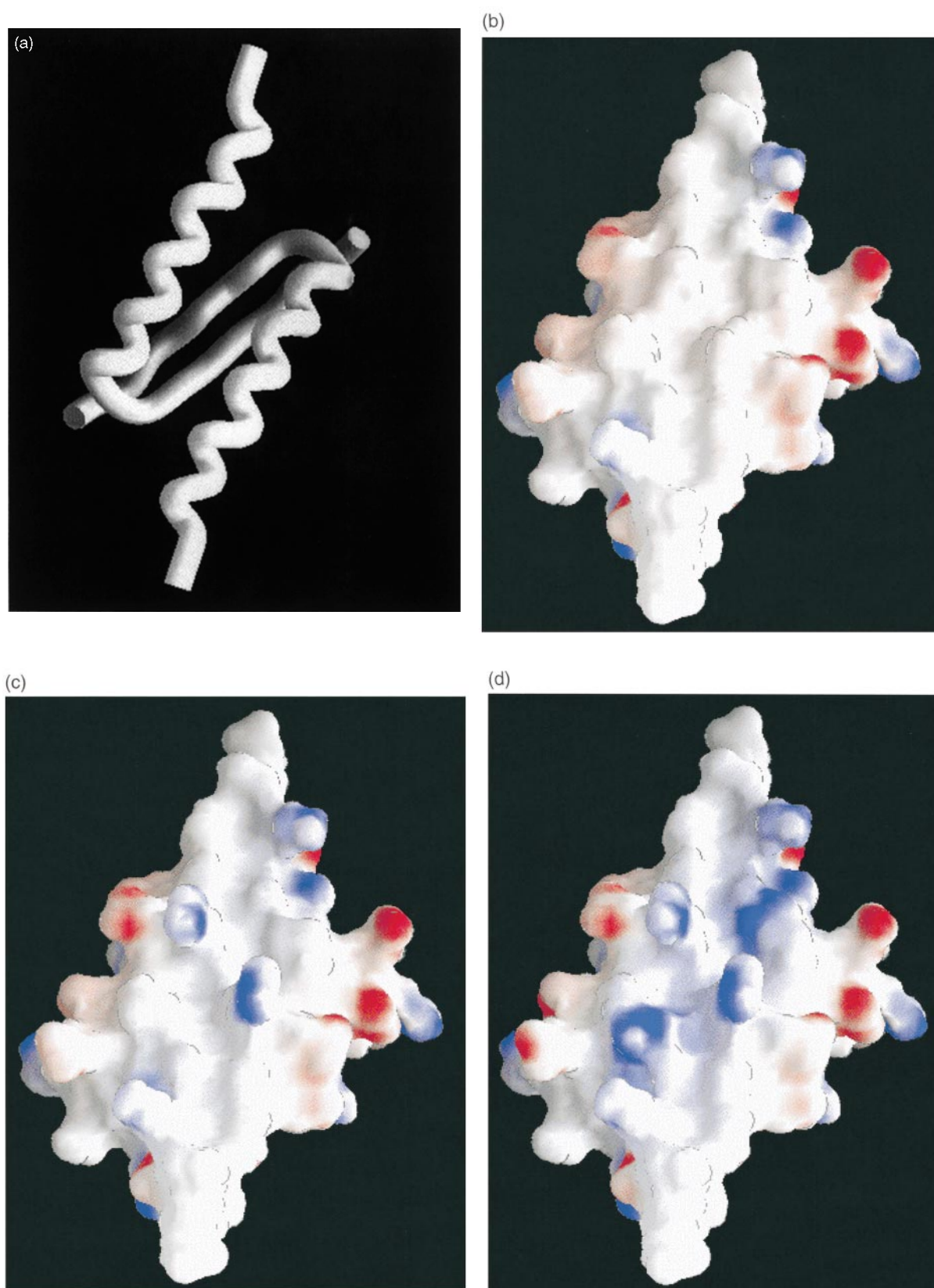


Figure 1. (a) A backbone worm diagram of the 3D structure of the WT p53 oligomerization domain.³² For clarity, only one of the dimeric subunits is shown. (b) A surface potential representation of the non-polar (white) and polar (red and blue) surfaces of half of the p53 tetramer structure is shown with the dimerization interface exposed in the same orientation as shown in (a). The expected disruptions of the hydrophobic dimerization interface (white) *via* the introduction of a polar side-chain (red) at position (c) 344, or (d) both 340 and 344 are depicted. Diagrams were generated using the program GRASP⁶⁹ with the surface potential ranging from -25.1 kT to 25.1 kT .

Table 1. Biophysical characterization of p53 oligomeric mutants at positions 340 and/or 344

Protein	Aggregates (%)	t_m (°C) ^a	Oligomeric state
WT	<5	85 ^d	Tetramer
R337C ^c	65-75	33 ^c	Tetramer/dimer/monomer ^c
M340H	45-55	58 ^b	Tetramer ^b
M340S	55-65	59 ^b	Tetramer ^b
M340 K	5-15	66 ^b	Tetramer ^b
M340Q	35-45	62 ^b	Dimer/tetramer ^b
M340E	45-55	34 ^b	Dimer/tetramer ^b
M340D	45-55	38 ^b	Dimer/tetramer ^b
L344P ^c	15-25	-	Monomer ^c
L344 K	5-15	48 ^b	Dimer ^b
L344R	5-15	43 ^b	Dimer ^b
L344Q	5-15	50 ^b	Dimer ^b
L344A	20-30	49 ^b	Dimer ^b
M340E/L344 K	<5	46	Dimer
M340Q/L344R	<5	35	Dimer

^a t_m values indicate the temperature at which the protein sample is half-folded and half-unfolded as measured by CD spectroscopy with 40-50 μ M protein samples.

^b Noolandi *et al.*³¹

^c Davison *et al.*³⁰

^d Johnson *et al.*⁴⁴

following the characteristic α -helical CD signal at 222 nm they all display a reduction in their resistance to thermal denaturation. Figure 2(b) shows the thermal melting curves for a subset of the mutants with their corresponding melting temperatures (t_m) summarized in Table 1. Analysis of post-thermal denaturation CD spectra indicates that each of the double and single-mutant proteins displays reversible denaturation with the exception of mutants Met340Asp and Met340Glu, both of which precipitate upon thermal denaturation (data not shown). Comparison of the melting curves reveals that mutation to a polar or charged residue at position 344 produces proteins with comparable with t_m values in the range of 43 to 49 °C, while similar substitutions at position 340 produce mutants with a wide range of t_m values. The double mutants MQLR and MELK have t_m values of 35 and 46 °C, respectively. It is interesting to note that the t_m of MQLR (35 °C) is less than the t_m values of each of the respective single-mutants Met340Gln (62 °C) and Leu344Arg (43 °C), while the t_m of MELK (46 °C) is between that of Met340Glu (34 °C) and Leu344Lys (48 °C). This suggests that a stabilizing interaction is occurring between Glu340 and Lys344, which are a single helical-turn away from one another.

NMR structure of MQLR dimeric mutant

It is apparent from the above experiments that the double mutants MQLR and MELK were the only proteins studied that are solely dimeric and capable of attaining concentrations ≥ 1.5 mM without aggregation, and were thus suitable for NMR structural analysis. Due to its extremely high expression rate with yields of ~ 80 mg/l, MQLR was chosen as the final candidate for structure determination.

NMR chemical shift values reflect the local environment of each nucleus and are sensitive to changes in the protein conformation. Consequently, the formation of free dimers in solution alters the chemical shifts of the residues along the newly exposed dimer-dimer interface of MQLR (Figure 3). It is also evident from these values that the residues in the β -sheet and turn exist in much the same conformation and environment as in the WT p53tet structure.

The solution structure of MQLR is a symmetric dimer that is essentially half of the WT p53tet structure, and maintains the same secondary and tertiary structures and side-chain packing in the dimer core, as intended (Figure 4). Backbone and all heavy atoms within the structured regions (residues 326-354) of the 20 lowest energy structures align with an rms deviation from the mean of 0.48 and 1.78 Å, respectively. The hydrophobic side-chains buried between the β -sheet and α -helices retain the same packing as the WT side-chains, with an rms deviation of 0.47 Å amongst the heavy atoms of the core residues Phe328, Leu330, Ile332, Phe341 and Leu348. The most significant differences between the dimer and half-tetramer occur at the C-terminal ends of the α -helices. While the helices of WT p53tet are quite stable and linear, residues 352-356 of MQLR are more open and flexible (Figure 5), since they lack the stabilizing interactions that are contributed by the opposing dimer in the WT structure.

Functional activities of p53 mutants with altered oligomeric states

Two well-characterized functions of p53 include the ability to promote transcription of genes that contain a p53-responsive element and the ability to block progression of the cell cycle from G₁ to S. In

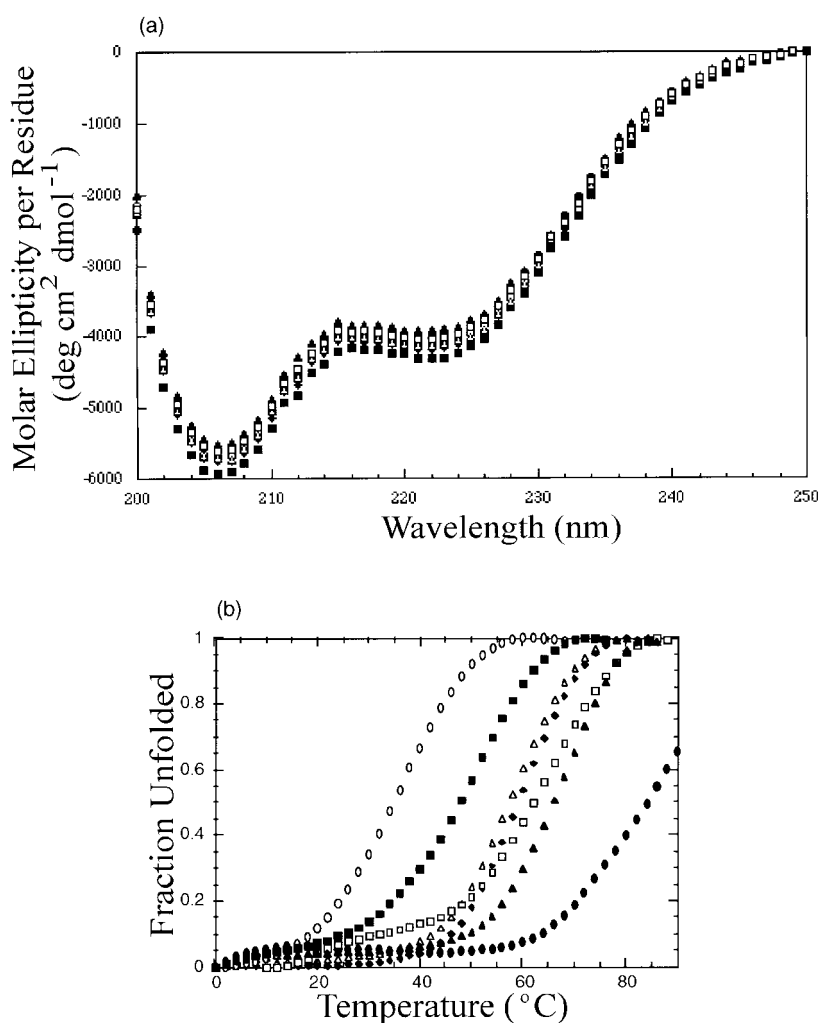


Figure 2. (a) Far-UV circular dichroism (CD) spectra at 25 °C, and (b) thermal denaturation (monitored $[\theta]_{222}$) of residues 310-360 19b for WT (filled circle), and mutants Met340Ser (filled diamond), Met340His (triangle), Met340Gln (square), Met340Lys (filled triangle), Met340Gln/Leu344Arg (circle), and Leu344Lys (filled square) with monomer concentrations of 40-50 μ M. The ellipticity values were normalized for protein concentration in (a). The corresponding spectra indicate that the relative amount of secondary structure for each mutant is comparable to that of WT. The temperature dependence of the α -helical signal in (b) is plotted as a fraction of unfolded protein assuming each protein is fully folded at 4 °C and completely unfolded when there was no further change in the CD signal with increasing temperature.

order to assess the role that oligomerization plays in these activities of p53, three full-length mutants that span a range of oligomeric states were selected for cell-cycle arrest and transcriptional transactivation assays. The oligomeric forms of the chosen mutants include a destabilized tetramer (Met340Lys₁₋₃₉₃), a dimer (MQLR₁₋₃₉₃) and a monomer (Leu344Pro₁₋₃₉₃).

SAOS2 cells, which harbor a homozygous deletion of the p53 gene locus and do not produce p53 protein, were transfected with expression plasmids encoding WT or oligomeric mutant forms of p53. Two days after transfection, cells were fixed, stained for p53 and subjected to cell-cycle analysis as determined by flow cytometry. Only the successfully transfected, p53-positive cells were included in the cell-cycle analysis. WT p53-induced cell-cycle arrest is characterized by a distinct obstruction of G₁/S phase progression,^{35,36} resulting in a depletion of cells in S phase with a subsequent accumulation of cells in G₁ phase. The p53tet mutant that is capable of forming tetramers (Met340Lys₁₋₃₉₃) is able to block G₁/S progression as well as WT p53₁₋₃₉₃ (Figure 6(a)). However,

dimeric and monomeric p53tet mutants exhibit only a marginal ability to affect the cell-cycle population distribution, an effect similar to the tumor-derived DNA-binding mutant His175Arg.

To determine whether monomers and dimers retained transactivation activity, transient expression studies were performed with the luciferase reporter plasmid (p21P-luc) in which the human p21^{WAF1} promoter containing a resident p53-responsive element was linked upstream of a luciferase coding sequence. SAOS2 cells were co-transfected with the luciferase reporter and expression plasmids encoding WT or oligomeric mutant forms of p53. In this assay the activity of each p53tet₁₋₃₉₃ mutant correlates with oligomeric state where monomers (Leu344Pro₁₋₃₉₃), dimers (MQLR₁₋₃₉₃) and tetramers (WT p53tet₁₋₃₉₃ and Met340Lys₁₋₃₉₃) display roughly background, half, and full activity, respectively (Figure 6(b)).

Discussion

Based on the known 3D structure of the WT p53tet domain³² we have generated a set of oligo-

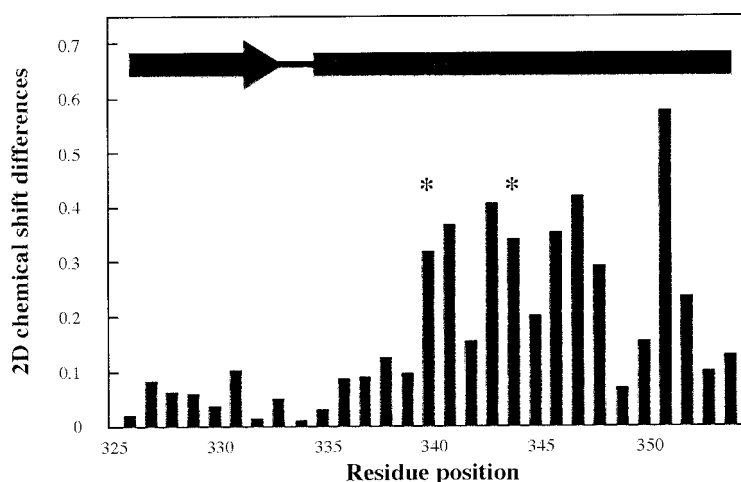


Figure 3. Comparison of the chemical shifts of backbone amide (N and HN) resonances of the p53-MQLR and WT p53tet oligomerization domains. The chemical shift perturbation vector was calculated from the absolute value of the chemical shift differences. A scaling factor was used for the ^{15}N nuclei derived from the average standard deviation for backbone chemical shifts over all non-proline residues from the BioMagResBank chemical shift database (<http://www.bmrb.wisc.edu/>). The backbone chemical shift vector was calculated as follows:

$$\Delta^{2\text{D}} = [(\Delta^{\text{HN}})^2 + (\Delta^{\text{NR}^{\text{N}}})^2]^{1/2}$$

where $R^{\text{N}} = 0.154$, and Δ^{HN} , and Δ^{N} are the chemical shift differences for backbone resonances of each residue between MQLR and WT p53tet. The secondary structure for the corresponding residues is indicated with an arrow and rectangle representing the β -sheet and α -helical regions, respectively. The location of each mutation is marked with a star for clarity. The magnitude of chemical shift changes is minimal within the β -sheet and turn regions, while more significant changes are apparent throughout the α -helical regions in the proximity of the point mutations.

meric single³¹ and double mutants, through hydrophilic substitution at the hydrophobic dimer-dimer interface, in order to determine the role that oligomerization plays in the functions of p53. As shown in the analysis of an alanine scanning mutagenesis analysis performed by Mateu & Fersht,²⁶ residues Met340 and Leu344 are central to the assembly of the tetramerization domain, with alterations at position 344 affecting the oligomeric state more significantly. Here, mutations involve the incorporation of full and/or partial charges into the dimer-dimer interface. The impact of mutations at position 344 in terms of oligomeric state can be rationalized by noting that the proximity of these side-chains to one another is much closer in the tetramer than those at position 340. The resulting charge repulsion experienced at the dimer-dimer interface due to substitutions at position 344 would thus be greater than that at position 340.³¹ Accordingly, a single polar substitution at position 344 results in a dimeric form of p53, while substitution at position 340 is insufficient to completely inhibit tetramerization, yielding destabilized tetramers or dimer-tetramer equilibrium mixtures. Moreover, with the exception of Met340Lys, polar substitution at position 340 results in mutants that display a strong tendency to aggregate non-specifically. This is most likely because the resultant dimer-dimer interface still contains a significant hydrophobic patch that would exhibit a high propensity to interact with other non-polar protein surfaces.

The p53tet double mutants containing substitutions at positions 340 and 344 produced dimers that were suitable for structure analysis. Unlike the dimeric p53 mutant Met340Lys/Phe341Ile/Leu344-Tyr reported by McCoy *et al.*,³⁷ which has parallel α -helices, and the chimeric p53 protein containing a parallel leucine-zipper dimerization domain substituted for the WT oligomerization domain,³⁸ our double mutant, MQLR, forms a dimer that resembles a Wtp53 "half-tetramer". Thus, MQLR retains the WT p53tet N and C-terminal orientations in addition to many of the surface properties of the WT oligomerization domain. These properties may be important for orientation of the other p53 domains in the context of full-length MQLR as well as potential protein-protein interactions occurring with the oligomerization domain.^{39,40}

When we compared the *in vivo* activities of full-length p53 oligomeric mutants with Wtp53 and negative controls, we found a direct correlation between the amount of transcriptional transactivation activity and oligomeric state, with monomers and dimers capable of background and roughly half activity, respectively. Functional cell-cycle arrest, however, requires proteins capable of forming a tetramer. It is interesting to note that Met340Lys, which exists as destabilized tetramer behaved better than WT in the two *in vivo* assays. The literature indicates that mutant p53 proteins with mixed oligomeric states exhibit variable functionality in a number of *in vivo* assays. For



Figure 4. Superposition of the ensemble average of the 20 lowest energy structures of p53 MQLR (black) with the ensemble average of the WT half-tetramer (grey). The two structures show significant similarity throughout the β -sheet, turn, and N-terminal portions of the α -helices with a backbone rmsd of 0.79 Å across residues 327-348 inclusively. The C-terminal ends of the p53-MQLR dimer stray from the WT form with a backbone rms deviation of 2.84 Å between the two structures throughout residues 349-356.

example, in a study of tumor-derived mutants found within the oligomerization domain,⁴¹ the mutants Leu330His, Arg337Leu and Arg337Cys displayed a dose-dependent transcriptional activity. Furthermore, in another study, the oligomeric mutant Lys351stop, which exists as both dimers and tetramers²¹ was found to be deficient in cell-cycle arrest assays, retained 40% of WTp53 transactivation activity, yet performed better than WTp53 at growth inhibition in SAOS2 cells.¹⁷ Interestingly, the only other mutant that has been confirmed to exist in multiple oligomeric states is Arg337Cys³⁰ and it also shows variable defects relative to WT activities.^{28,42} These results suggest that p53 oligomeric mutants that exist in concentration-dependent, multiple oligomeric states may display variable functional defects, compared to WT, depending on the assay and protein concentration.

In addition to a reduced ability to bind DNA targets, the functional defects of oligomeric mutants may be in part due to an alteration in interactions with other cellular proteins. For example, proteins such as tms1⁴⁰ and p34^{cdc2}³⁹ interact with the p53tet domain. Furthermore, Lomax *et al.*⁴² have shown that the oligomeric mutants Leu344Pro₁₋₃₉₃ and Arg337Cys₁₋₃₉₃ display a reduced ability to

bind to MDM2, a protein which regulates p53 stability and activity through a negative feedback loop. The ability to separate the *in vivo* activities of p53 by altering the oligomeric state may prove to be a useful tool for deciphering the multiple cellular roles of p53.

Materials and Methods

Plasmid preparation and protein purification

The DNA sequence encoding residues 310-360 of WT human p53 was subcloned into the pET15b and pET19b vectors (Novagen Inc.) using standard techniques.⁴³ The resulting plasmid, pET-p53(310-360)15b(19b), expresses six (ten) histidine residues followed by a linker containing a thrombin (enterokinase) cleavage site and a His-Met dipeptide immediately N-terminal to the p53 sequence. The p53 mutations at either Met340 or Leu344 were created by oligonucleotide-directed mutagenesis on pET-p53(310-360)15b using the Quick-Change mutagenesis kit (Stratagene), and subsequently verified by DNA sequence analysis. Mutant plasmids were further subcloned into the pET19b vector. Recombinant His-tagged proteins were expressed and purified by nickel affinity chromatography, and cleaved from the poly-histidine tag by thrombin or enterokinase digestion.^{32,44} The yield of purified protein was 5-80 mg/l of culture. Samples were then dialyzed twice for 24 hours at 4°C against four liters of buffer (25 mM sodium phosphate, 100-150 mM NaCl, pH 7.0) using Spectra/por 3500 molecular mass cut-off dialysis membrane. Proteins were then concentrated by ultrafiltration using Centricon-3 membranes (Amicon). Final stock protein concentrations were determined using the extinction coefficient $\epsilon_{275} = 1475 \text{ M}^{-1} \text{ cm}^{-1}$ per solvent-exposed tyrosine residue in unfolding conditions of 6.5 M guanidine-HCl.

Circular dichroism

Far-UV CD spectra were recorded on an Aviv 62A DS circular dichroism spectrometer equipped with a thermoelectric temperature controller. Measurements were made at 25°C using a 0.1 cm cuvette at a sample concentration of 40-50 μM (monomer) in a buffer of 25 mM sodium phosphate, 150 mM NaCl, pH 7.0. Ellipticity at 222 nm was monitored as a function of temperature every 3 deg. C, allowing four minutes for sample equilibration and a signal average of 99 seconds for each data point following thermal unfolding. Melting temperatures (t_m) were assigned to the midpoint of the fraction of unfolded protein (F_U) as determined by the relationship:

$$F_U(\theta) = (\theta - \theta_N) / (\theta_U - \theta_N)$$

where θ is the ellipticity at a given temperature, θ_N and θ_U represent the ellipticity values at temperatures where the protein is fully folded or unfolded, respectively.

NMR spectroscopy and spectral assignments

All spectra were recorded at 25°C on either a Varian Unity Plus 500-MHz or Unity 600-MHz spectrometer equipped with pulse-field gradient units and actively

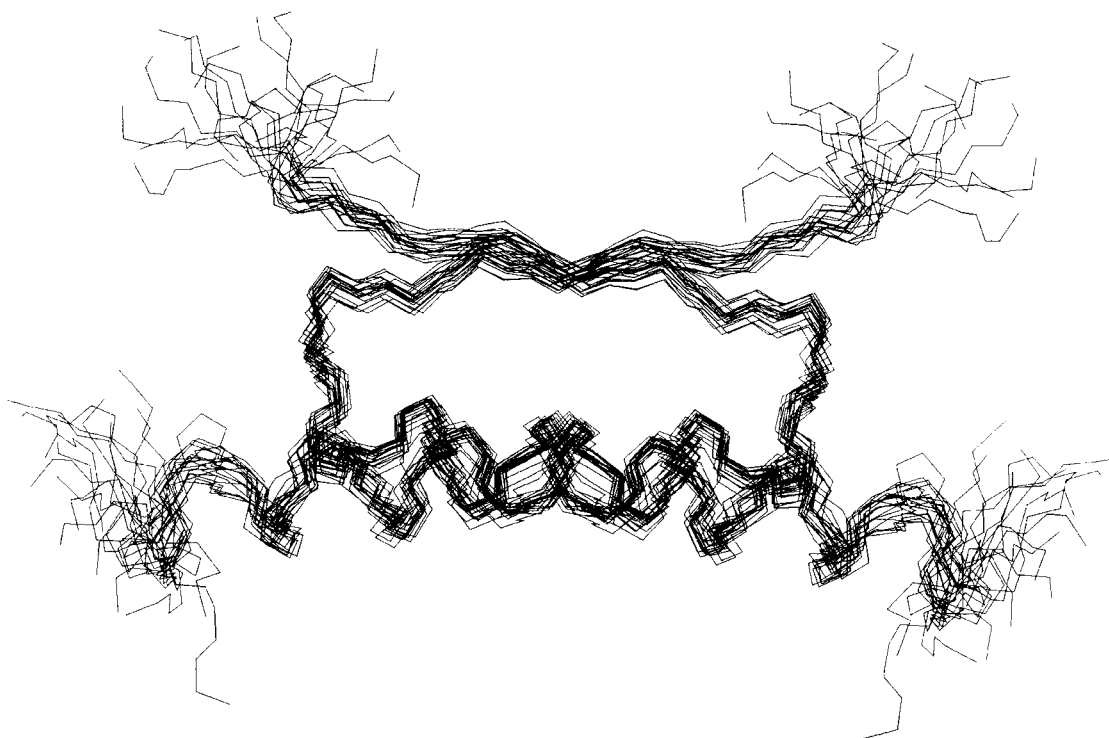


Figure 5. A backbone trace of the family of 20 lowest energy structures superimposed in order to minimize the root-mean-square deviation of the main-chain backbone atoms. Note the lack of convergence at the C-terminal ends of the helices.

shielded z-gradient triple-resonance probes. NMR experiments involving correlations of amide protons were conducted with gradient enhanced versions⁴⁵ of the original pulse sequences. NMR data used in these studies were processed with nmrPipe software.⁴⁶ Spectral analysis was achieved with the programs PIPP and CAPP,⁴⁷ and NMRView.⁴⁸ Sequential assignment of ¹H, ¹⁵N, ¹³C^α, and ¹³C^β resonances for the globular domain (residues 325–355) was achieved based on the following 3D NMR experiments: ¹⁵N-NOESY-HSQC,⁴⁹ HNCA,⁵⁰ HNCACB,⁵¹ (HB)CBCA(CO)NNH,⁵² and a ¹H-¹⁵N heteronuclear single quantum correlation (HSQC)^{53,54} spectra. Side-chain ¹³C and ¹H resonances of aliphatic residues of p53-MQLR were assigned from the following 3D and 2D spectra: HCCH-TOCSY⁵⁵ recorded with a mixing time (τ_m) of 7 ms, CCC-TOCSY,⁵⁶ 2D constant time ¹³C-HSQC,⁵⁷ ¹⁵N TOCSY-HSQC⁵⁸ with a τ_m of 62 ms, and an HNHA.⁵⁹ Side-chain ¹H resonances of aromatic residues were assigned from 100 ms τ_m homonuclear 2D NOESY⁶⁰ and TOCSY⁶¹ spectra performed in ²H₂O. ¹H-¹H nuclear Overhauser effects (NOEs) were then identified from the following spectra: ¹³C-edited NOESY in ²H₂O,⁶² ¹³C, ¹⁵N-edited NOESY in H₂O⁶³ with NOE of τ_m of 150 ms, and 2D homonuclear NOESY in ²H₂O to identify NOEs involving aromatic residues. Finally, ³J_{NH-H α} coupling constants were determined using HNHA.⁵⁹ Spectral assignments have been deposited in the BioMagResBank (BMRB) under the accession number 4934.

Structural restraints and calculations

The NMR-derived structural information used to calculate the structure of the p53-MQLR dimer included three types of restraints. (i) Based on cross-peak intensities, NOE data was used to determine hydrogen-hydro-

Table 2. Structural statistics for the 20 lowest energy simulated annealing structures of p53 MQLR

rms deviation from distance restraints (Å)	
All (495) ^a	0.008 ± 0.0008
Intra-residue ($i = j$) (57)	0.004 ± 0.001
Sequential ($ i - j = 1$) (163)	0.007 ± 0.002
Medium ($1 < i - j \leq 4$) (119)	0.007 ± 0.002
Long ($ i - j > 4$) (124)	0.005 ± 0.002
rms deviation from angle restraints (deg.)	
Dihedral (24)	0.195 ± 0.005
rms deviation from covalent geometry	
Bond lengths (Å)	0.0008 ± 0.0004
Angles (deg.)	0.442 ± 0.002
Improper (deg.)	0.308 ± 0.004
Residues in most favorable region of Ramachandran plot ^b (%)	89.4 ± 2.9

^a The number of each type of restraint is given in parentheses.

^b Assessed using the program PROCHECK⁷⁰ assuming a 2.0 Å resolution structure equivalent. Two residues in the ensemble of 20 structures have ϕ/ψ angles in the disallowed region of the Ramachandran map.

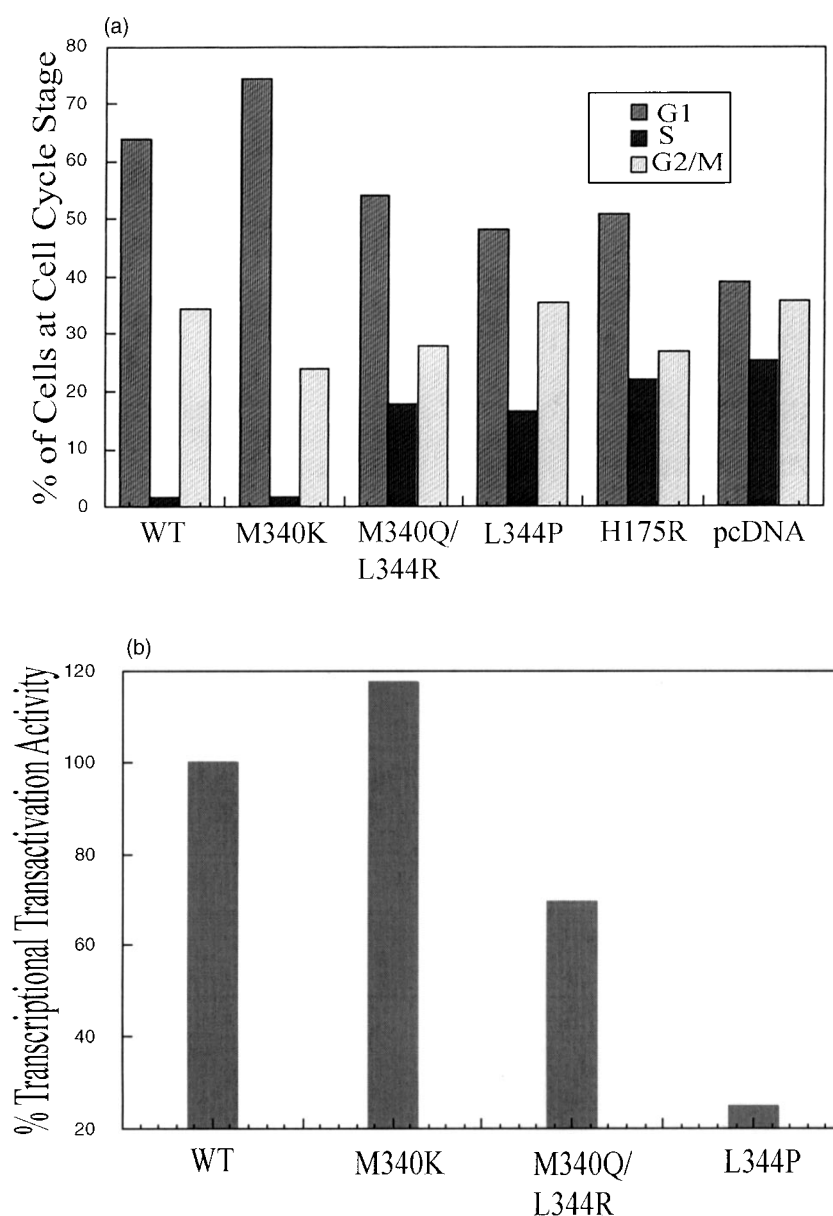


Figure 6. Functional characterization of full-length p53 oligomeric mutants. (a) Distribution of cells in each phase of the cell cycle after p53 expression. SAOS2 cells were transfected with p53 cDNAs encoding WTp53, p53His175Arg, oligomeric mutants and an empty vector control, pcDNA3. Forty-eight hours after transfection, cells were stained for p53 and p53-positive cells were selected for cell-cycle analysis using flow cytometry. Representative data from a single transfection experiment are shown. (b) Transcriptional activation of a p53-responsive promoter in transfected SAOS2 cells. SAOS2 cells were transfected with the p21 promoter-luciferase reporter plasmid (p21P-luc) and one of several p53pCDNA plasmids (WTp53₁₋₃₉₃ or oligomeric mutants) in which expression was controlled by the CMV promoter. Luciferase activity was measured in duplicate on two separate samples, 48 h after transfection using a luminometer and normalized for differences in the amount of expressed p53 protein determined by Western immuno-blotting as described in Materials and Methods. Mean values of percentage activity relative to WTp53 are shown for a single transfection experiment. The error is approximately 10% in each case.

gen distances which were classified into the four classes of strong, medium, weak and very weak with corresponding distance restraints of 1.7-2.8, 1.8-3.5, 1.8-5.0, and 1.8-6.0 Å, respectively. Pseudo-atom corrections were made to distance upper bounds involving methyl, methylene, and aromatic ring groups.⁶⁴ (ii) The ϕ angles of residues with $^3J_{\text{NH-H}\alpha}$ coupling constants greater than 8.0 Hz were constrained to $-120(\pm 40)^\circ$ while residues

with $^3J_{\text{NH-H}\alpha}$ values less than 5.5 Hz were constrained to ϕ angles of $-60(\pm 30)^\circ$. (iii) Main-chain hydrogen bond restraints (H-O, 2.5 Å; N-O, 3.5 Å) within α -helices and (H-O, 1.8-2.4 Å; N-O, 2.7-3.3 Å) for the β -sheet were implemented for residue pairs that were clearly structurally defined by characteristic NOE patterns of α -helices and β -sheets and appropriate $^3J_{\text{NH-H}\alpha}$ values. A total of 495 restraints were found (Table 2). Of the 124 long-

range distance restraints, 98 were intermolecular restraints that defined the quaternary structure of the dimer.

Three-dimensional structures were calculated by using the dynamic simulated annealing protocol⁶⁵ implemented within X-PLOR.⁶⁶ Monomer structures, generated with extended backbone dihedral angles, were used as starting points for structure calculations. Dimers were generated by duplication of the monomer coordinates. The X-PLOR non-crystallographic symmetry (NCS) parameter was employed to maintain symmetry between the monomer chains within each structure, while the symmetry pseudo-NOE term was used to maintain symmetrical inter-monomer contacts as described.⁶⁷ Initial calculations employed approximately seven unambiguous restraints per residue. Structures were calculated iteratively in order to resolve ambiguities in the identity of further NOEs through inspection of resultant structures. From a total of 50 simulated annealing structures calculated, the 20 lowest energy structures were selected. Structural statistics from this ensemble are listed in Table 2. There were no violations greater than 0.2 Å for distance restraints or 5° for angles.

Protein Data Bank accession numbers

The structural restraints and 20 lowest energy structures were deposited in the Research Collaboratory for Structural Bioinformatics (RCSB) Protein Data Bank (PDB) under the accession numbers RCSB:012556 and 1HS5 respectively.

Cell culture and transfection

SAOS2 cells were cultured in α -MEM with 10% (v/v) fetal bovine serum at 37°C in a humidified atmosphere of 5% CO₂ in air. Cells in 60 mm dishes were transfected with plasmids using the lipofectin reagent (Gibco) in the absence of serum and antibiotics. The DNA-lipofectin mixture was left on the cells for five hours at 37°C. Cells were then cultured in complete growth medium for 48 hours at 37°C prior to analysis.

Cell cycle analysis

For the cell-cycle analysis, the cells were washed in PBS, treated with trypsin and collected by centrifugation. Cells were fixed in cold acetone/methanol (30:70, v/v) for ten minutes at -20°C, spun, rinsed with cold PBS, resuspended in PBS containing 0.5% (w/v) BSA and primary antibodies against p53 (PAb122 and PAb1801), and incubated for 30 minutes at room temperature. Cells were rinsed, resuspended in PBS containing 0.5% BSA and secondary antibody (fluorescein isothiocyanate-conjugated rabbit anti-mouse immunoglobulin G), and incubated at room temperature in the dark for 30 minutes. Cells were rinsed, resuspended in PBS containing 0.5% BSA, RNase A (1 mg/ml) and propidium iodide (10 µg/ml), and incubated at room temperature for 30 minutes. The stained cells were analysed on a FACScan flow cytometer (Becton Dickinson) using the Lysis II software program and the distribution of cells in the cell cycle was determined with ModFitLT. Cells exhibiting high p53 fluorescence intensity (FITC), representing the successfully transfected sub-population, were selected by gating. Equal numbers of FITC-positive (p53+) and

FITC-negative (untransfected) cells were assessed for cell cycle distribution as defined by DNA content on the basis of propidium iodide staining intensity. Debris and cell doublets were excluded on the basis of forward and side light-scattering properties. In all cases the cell cycle profile of the transfected (p53+) cells was compared to the cell cycle profile of the untransfected cells (p53-) within the same population. The latter always resembled the cells transfected with the pCDNA vector alone.

Luciferase assay

For the luciferase assay, cells were transfected with p21P-luc,⁶⁸ a luciferase reporter plasmid under the control of the p53-responsive p21^{WAF1} promoter, together with plasmids expressing WT or mutant p53. Forty-eight hours after transfection, the cells were collected and distributed equally into two Eppendorf tubes. One sample was used for Western blotting to determine the amount of p53 expressed in the cells and the second sample was used to determine the amount of luciferase activity. For Western blotting, the cells were lysed by boiling for five minutes in SDS lysis buffer (0.1 M Tris (pH 6.8), 4% (w/v) SDS, 20% (w/v) glycerol) and the proteins were resolved by SDS-polyacrylamide gel electrophoresis. The protein concentration in the cell lysates was determined using a modified Lowry assay (Sigma). Proteins were transferred to PVDF membranes and p53 protein was detected with the p53-specific antibody PAb1801 followed with a secondary sheep anti-mouse immunoglobulin G that was conjugated to horseradish peroxidase. The p53-antibody complex was detected by enhanced chemiluminescence (Mandel).

Luciferase activity was measured in duplicate on two separate samples using the luciferase assay reagent (Promega) as described by the manufacturer. Cells were lysed using the cell lysis reagent (Promega) and total protein concentration in the cell extracts was determined using the Bio-Rad protein assay with BSA as the standard. Luciferase activity was measured on a Berthold LB9507 luminometer using sample volumes that contained the same amount of p53 protein. The intensity of light emission was measured over a five second interval.

Acknowledgments

We thank Les Hicks and Peter Yin for excellent technical assistance. This research was supported by the National Cancer Institute of Canada (C.H.A. and S.B.), with funds from the Terry Fox Run.

References

1. Picksley, S. M. & Lane, D. P. (1994). p53 and Rb: their cellular roles. *Curr. Opin. Cell. Biol.* **6**, 853-858.
2. Zambetti, G. P. & Levine, A. J. (1993). A comparison of the biological activities of wild-type and mutant p53. *FASEB J.* **7**, 855-865.
3. El-Deiry, W. S., Tokino, T., Velculescu, V. E., Levy, D. B., Parsons, R., Trent, J. M., Lin, D., Mercer, W. E., Kinzler, K. W. & Vogelstein, B. (1993). WAF1, a potential mediator of p53 tumor suppression. *Cell*, **75**, 817-825.

4. Harper, J. W., Adam, G. R., Wei, N., Keyomarsi, K. & Elledge, S. J. (1993). The p21 Cdk-interacting protein Cip1 is a potent inhibitor of G1 cyclin-dependent kinases. *Cell*, **75**, 805-816.
5. Kastan, M. B., Zhan, Q., El-Deiry, W. S., Carrier, F., Jacks, T., Walsh, W. V., Plunkett, B. S., Vogelstein, B. & Fornace, A. J., Jr (1992). A mammalian cell cycle checkpoint pathway utilizing p53 and GADD45 is defective in ataxia-telangiectasia. *Cell*, **71**, 587-597.
6. Xiong, Y., Hannon, G. J., Zhang, H., Casso, D., Kobayashi, R. & Beach, D. (1993). p21 is a universal inhibitor of cyclin kinases. *Nature*, **366**, 701-704.
7. Polyak, K., Xia, Y., Zweier, J., Kinzler, K. & Vogelstein, B. (1997). A model for p53-induced apoptosis. *Nature*, **389**, 300-305.
8. Miyashita, T. & Reed, J. C. (1995). Tumor suppressor p53 is a direct transcriptional activator of the human bax gene. *Cell*, **80**, 293-299.
9. Donehower, L. A. & Bradley, A. (1993). The tumor suppressor p53. *Biochim. Biophys. Acta*, **1155**, 181-205.
10. Ko, J. L. & Prives, C. (1996). p53: puzzle and paradigm. *Genes Dev.* **10**, 1054-1072.
11. Levine, A. J. (1997). p53, the cellular gatekeeper for growth and division. *Cell*, **88**, 323-331.
12. Arrowsmith, C. H. & Morin, P. (1996). New insights into p53 function from structural studies. *Oncogene*, **12**, 1379-1385.
13. Cariello, N. F., Cui, L., Beroud, C. & Soussi, T. (1994). Database and software for the analysis of mutations in the human p53 gene. *Cancer Res.* **54**, 4454-4460.
14. Hollstein, M., Sidransky, D., Vogelstein, B. & Harris, C. C. (1991). p53 mutations in human cancers. *Science*, **253**, 49-53.
15. Hollstein, M., Shimer, B., Greenblatt, M., Soussi, T., Hovig, E., Montesano, R. & Harris, C. C. (1996). Somatic point mutations in the p53 gene of human tumors and cell lines: updated compilation. *Nucl. Acids Res.* **24**, 141-146.
16. Soussi, T. & May, P. (1996). Structural aspects of the p53 protein in relation to gene evolution: a second look. *J. Mol. Biol.* **260**, 623-637.
17. Ishioka, C., Englert, C., Winge, P., Yan, Y.-X., Engelstein, M. & Friend, S. (1995). Mutational analysis of the carboxy-terminal portion of p53 using both yeast and mammalian cell assays *in vivo*. *Oncogene*, **10**, 1485-1492.
18. Hann, B. C. & Lane, D. P. (1995). The dominating effect of mutant p53. *Nature Genet.* **9**, 221-222.
19. Jeffery, P. D., Gorina, S. & Pavletich, N. P. (1995). Crystal structure of the tetramerization domain of the p53 tumor suppressor at 1.7 angstroms. *Science*, **267**, 1498-1502.
20. Waterman, J. L. F., Shenk, J. L. & Halazonetis, T. D. (1995). The dihedral symmetry of the p53 tetramerization domain mandates a conformational switch upon DNA binding. *EMBO J.* **14**, 5182-5191.
21. Ishioka, C., Englert, C., Shimada, A., Osada, M., Jia, J.-Q., Suzuki, T., Gamo, M. & Kanamura, R. (1997). Oligomerization is not essential for growth suppression by p53 in p53-deficient osteosarcoma Saos-2 cells. *Biochem. Biophys. Res. Commun.* **232**, 54-60.
22. Slingerland, J. M., Jenkins, J. R. & Benchimol, S. (1993). The transforming and suppressor functions of p53 alleles: effects of mutations that disrupt phosphorylation, oligomerization and nuclear translocation. *EMBO J.* **12**, 1029-1037.
23. Tarunina, M. & Jenkins, J. R. (1993). Human p53 binds DNA as a protein homodimer but monomeric variants retain full transcription transactivation activity. *Oncogene*, **8**, 3165-3173.
24. Harvey, M., Vogel, H., Morris, D., Bradley, A., Bernstein, A. & Donehower, L. A. (1995). A mutant p53 transgene accelerates tumour development in heterozygous but not nullizygous p53-deficient mice. *Nature Genet.* **9**, 305-311.
25. Shaulian, E., Zauberman, A., Ginsberg, D. & Oren, M. (1992). Identification of a minimal transforming domain of p53: negative dominance through abrogation of sequence-specific DNA binding. *Mol. Cell. Biol.* **12**, 5581-5592.
26. Mateu, M. G. & Fersht, A. R. (1998). Nine hydrophobic side-chains are key determinants of the thermodynamic stability and oligomerization status of tumour suppressor p53 tetramerization domain. *EMBO J.* **17**, 2748-2758.
27. Varley, J. M., McGowan, G., Thorncroft, M., Cochrane, S., Morrison, P., Woll, P., Kelsey, A. M., Mitchell, E. L. D., Boyle, J., Birch, J. M. & Evans, D. G. R. (1996). A previously undescribed mutation within the tetramerisation domain of TP53 in a family with Li-Fraumeni syndrome. *Oncogene*, **12**, 2437-2442.
28. Lomax, M. E., Barnes, D. M., Gilchrist, R., Picksley, S. M., Varley, J. M. & Camplejohn, R. S. (1997). Two functional assays employed to detect an unusual mutation in the oligomerisation domain of p53 in a Li-Fraumeni like family. *Oncogene*, **14**, 1869-1974.
29. Bell, D. W., Varley, J. M., Szydlo, T. E., Kang, D. H., Wahrer, D. C., Shannon, K. E., Lubratovich, M., Verselis, S. J., Isselbacher, K. J., Fraumeni, J. F., Birch, J. M., Li, F. P., Garber, J. E. & Haber, D. A. (1999). Heterozygous germ line hCHK2 mutations in Li-Fraumeni syndrome. *Science*, **286**, 2528-2531.
30. Davison, T. S., Yin, P., Nie, E., Kay, C. & Arrowsmith, C. H. (1998). Characterization of the oligomerization defects of two p53 mutants found in families with Li-Fraumeni and Li-Fraumeni-like syndrome. *Oncogene*, **17**, 651-656.
31. Noolandi, J., Davison, T. S., Volkel, A. R., Nie, X.-F., Kay, C. & Arrowsmith, C. H. (2000). A meanfield approach to the thermodynamics of a protein-solvent system with application to the oligomerization of the tumor suppressor p53. *Proc. Natl Acad. Sci. USA*, **97**, 9955-9960.
32. Lee, W., Harvey, T. S., Yin, Y., Yau, P., Litchfield, D. & Arrowsmith, C. H. (1994). Solution structure of the tetrameric minimum transforming domain of p53. *Nature Struct. Biol.* **1**, 877-890.
33. Clore, G. M., Onichiinski, J. G., Sakaguchi, K., Zambrano, N., Sakamoto, H., Appells, E. & Gronenborn, A. (1994). High-resolution structure of the oligomerization domain of p53 by multidimensional NMR. *Science*, **265**, 386-391.
34. Clore, G. M., Ernst, J., Clubb, R., Onichiinski, J. G., Kennedy, W. M. P., Sakaguchi, K., Appella, E. & Gronenborn, A. (1995). Refined solution structure of the oligomerization domain of the tumour suppressor p53. *Nature Struct. Biol.* **2**, 321-333.
35. Michalovitz, D., Halevy, O. & Oren, M. (1990). Conditional inhibition of transformation and of cell proliferation by a temperature-sensitive mutant of p53. *Cell*, **62**, 671-680.
36. Mercer, W. E., Shields, M. T., Amin, M., Sauve, G. J., Appella, E., Romano, J. W. & Ullrich, S. J. (1990). Negative growth regulation in a glioblastoma tumor

- cell line that conditionally expresses human wild-type p53. *Proc. Natl Acad. Sci. USA*, **87**, 6166-6170.
37. McCoy, M., Stavridi, E. S., Waterman, J. L. F., Wiczorek, A. M., Opella, S. J. & Halazonetis, T. D. (1997). Hydrophobic side-chain size is a determinant of the three-dimensional structure of the p53 oligomerization domain. *EMBO J.* **16**, 6230-6236.
 38. Waterman, M. J. F., Waterman, J. L. F. & Halazonetis, T. D. (1996). An engineered four-stranded coiled coil substitutes for the tetramerization domain of wild-type p53 and alleviates trans-dominant inhibition by tumor-derived p53 mutants. *Cancer Res.* **56**, 158-1163.
 39. Wagner, P., Fuchs, A., Gotz, C., Nastainczyk, W. & Montenarh, M. (1998). Fine mapping and regulation of the association of p53 with p34cdc2. *Oncogene*, **16**, 105-111.
 40. Wagner, P., Fuchs, A., Prowald, A., Montenarh, M. & Nastainczyk, W. (1995). Precise mapping of the tms1 binding site on p53. *FEBS Letters*, **377**, 155-158.
 41. Rollenhagen, C. & Chene, P. (1998). Characterization of p53 mutants identified in human tumors with a missense mutation in the tetramerization domain. *Int. J. Cancer*, **78**, 372-376.
 42. Lomax, M. E., Barnes, D. M., Gilchrist, R., Picksley, S. M., Varley, J. M. & Campjohn, R. S. (1998). Characterization of p53 oligomerization domain mutations isolated from LiFraumeni and LiFraumeni like family members. *Oncogene*, **17**, 643-649.
 43. Sambrook, J., Fritsch, E. F. & Maniatis, T. (1989). *Molecular Cloning*, 2nd edit., Cold Spring Harbor Laboratory Press, Cold Spring Harbor, NY.
 44. Johnson, C. R., Morin, P. E., Arrowsmith, C. H. & Freire, E. (1995). Thermodynamic analysis of the structural stability of the tetrameric oligomerization domain of p53 tumor suppressor. *Biochemistry*, **34**, 5309-5316.
 45. Kay, L. E., Keifer, P. & Saarinen, T. (1992). Pure absorption gradient enhanced heteronuclear single quantum correlation spectroscopy with improved sensitivity. *J. Am. Chem. Soc.* **114**, 10663-10665.
 46. Delaglio, F., Grzesiek, S., Vuister, G. W., Zhu, G., Pfeifer, J. & Bax, A. (1995). NMRPipe: a multidimensional spectral processing system based on UNIX pipes. *J. Biomol. NMR*, **6**, 277-293.
 47. Garrett, D. S., Powers, R., Gronenborn, A. M. & Clore, G. M. (1991). A common sense approach to peak picking in two-, three- and four-dimensional spectra using automatic computer analysis of contour diagrams. *J. Magn. Reson.* **95**, 214-220.
 48. Johnson, B. A. & Blevins, R. A. (1994). NMRView: a computer program for the visualization and analysis of NMR data. *J. Biomol. NMR*, **4**, 603-614.
 49. Marion, D., Kay, L. E., Sparks, S. W., Torchia, D. A. & Bax, A. (1989). Three-dimensional heteronuclear NMR of ¹⁵N labeled proteins. *J. Am. Chem. Soc.* **111**, 1515-1517.
 50. Kay, L. E., Ikura, M., Tschudin, R. & Bax, A. (1990). Three-dimensional triple resonance NMR spectroscopy of isotopically enriched proteins. *J. Magn. Reson.* **89**, 496-514.
 51. Wittekind, M. & Mueller, L. (1993). HNCACB, a high-sensitivity 3D NMR experiment to correlate amide-proton and nitrogen resonances with the alpha- and beta-carbon resonances in proteins. *J. Magn. Reson.* **169**, 949-961.
 52. Grzesiek, S. & Bax, A. (1992). Correlating backbone amide and side-chain resonances in larger proteins by multiple relayed triple resonance NMR. *J. Am. Chem. Soc.* **114**, 6291-6293.
 53. Bax, A. & Davis, D. G. (1985). Practical aspects of two-dimensional transverse NOE spectroscopy. *J. Magn. Reson.* **65**, 355.
 54. Bodenhausen, G. & Ruben, D. J. (1980). Natural abundance nitrogen-15 NMR by enhanced heteronuclear spectroscopy. *Chem. Phys. Letters*, **69**, 185-189.
 55. Bax, A., Clore, G. M. & Gronenborn, A. M. (1990). ¹H-¹H correlation via isotropic mixing of ¹³C magnetization: a new three-dimensional approach for assigning ¹H and ¹³C spectra of ¹³C-enriched proteins. *J. Magn. Reson.* **88**, 425-431.
 56. Montelione, G. T., Lyons, B. A., Emerson, S. D. & Tashiro, M. (1992). An efficient triple resonance experiment using carbon-13 isotropic mixing for determining sequence-specific resonance assignments of isotopically enriched proteins. *J. Am. Chem. Soc.* **114**, 10974-10975.
 57. Vuister, G. W. & Bax, A. (1992). Resolution enhancement and spectral editing of uniformly ¹³C enriched proteins by homonuclear broadband ¹³C-¹³C decoupling. *J. Magn. Reson.* **98**, 428-435.
 58. Marion, D., Driscoll, P. C., Kay, L. E., Wingfield, P. T., Bax, A., Gronenborn, A. M. & Clore, G. M. (1989). Overcoming the overlap problem in the assignment of ¹H NMR spectra of larger proteins by use of three-dimensional heteronuclear ¹H-¹⁵N Hartmann-Hahn-multiple quantum coherence and nuclear Overhauser-multiple quantum coherence spectroscopy: application to interleukin 1 beta. *Biochemistry*, **28**, 6150-6156.
 59. Vuister, G. W. & Bax, A. (1992). An empirical correlation between ¹J CaHa and protein backbone conformation. *J. Am. Chem. Soc.* **115**, 7772.
 60. Jeener, J., Meier, B. H., Backmann, P. & Ernst, R. R. (1979). Investigation of exchange processes by two-dimensional NMR spectroscopy. *J. Chem. Phys.* **71**, 4546-4553.
 61. Braunschweiler, L. & Ernst, R. R. (1983). Coherence transfer by isotropic mixing: application to proton correlation spectroscopy. *J. Magn. Reson.* **53**, 521-528.
 62. Ikura, M., Kay, L. E. & Bax, A. (1990). Three-dimensional NOESY-HMQC spectroscopy of a ¹³C-labeled protein. *J. Magn. Reson.* **86**, 204-209.
 63. Pascal, S. M., Muhandiram, D. R., Yamazaki, T., Forman-Kay, J. D. & Kay, L. E. (1994). Simultaneous acquisition of ¹⁵N- and ¹³C-Edited NOE spectra of proteins dissolved in H₂O. *J. Magn. Reson.* **B103**, 197-201.
 64. Wutrich, K., Billeter, M. & Braun, W. (1983). Pseudo-structures for the 20 common amino acids for use in studies of protein conformations by measurements of intramolecular proton-proton distance constraints with nuclear magnetic resonance. *J. Mol. Biol.* **169**, 949-961.
 65. Nilges, M., Gronenborn, A. M., Brunger, A. T. & Clore, G. M. (1988). Determination of three-dimensional structures of proteins by simulated annealing with interproton distance restraints. Application to crambin, potato carboxypeptidase inhibitor and barley serine proteinase inhibitor 2. *Protein Eng.* **2**, 27.
 66. Brunger, A. T. (1992). *A System for X-Ray Crystallography and NMR*, 3.1 edit., Yale University Press, New Haven, CT.

-
67. Nilges, M. (1993). A calculation strategy for the structure determination of symmetric dimers by ^1H NMR. *Proteins: Struct. Funct. Genet.* **17**, 295-309.
68. Vaziri, H., West, M. D., Allsopp, R. C., Davison, T. S., Wu, Y. S., Arrowsmith, C. H., Poirier, G. G. & Benchimol, S. (1997). ATM-dependent telomere loss in aging human diploid fibroblasts and DNA damage lead to the post-translational activation of p53 protein involving poly(ADP-ribose) polymerase. *EMBO J.* **16**, 6018-6033.
69. Nicholls, A., Sharp, K. A. & Honig, B. (1991). Protein folding and association: insights from the interfacial and thermodynamic properties of hydrocarbons. *Proteins: Struct. Funct. Genet.* **11**, 281-296.
70. Laskowski, R. A., Moss, D. S. & Thornton, J. M. (1993). Main-chain bond lengths and bond angles in protein structures. *J. Mol. Biol.* **231**, 1049-1067.

Edited by P. E. Wright

(Received 25 October 2000; received in revised form 3 January 2001; accepted 5 January 2001)